Theoretical and experimental evidence of level repulsion states and evanescent modes in sonic crystal stubbed waveguides

2012 New J. Phys. 14 023049

(http://iopscience.iop.org/1367-2630/14/2/023049)

New Journal of Physics
The open-access journal for physics

Theoretical and experimental evidence of level repulsion states and evanescent modes in sonic crystal stubbed waveguides

V Romero-García[1,4], J O Vasseur[2], L M Garcia-Raffi[3] and A C Hladky-Hennion[2]

[1] Instituto de Investigación para la Gestión Integrada de zonas Costeras, Universidad Politécnica de Valencia, Paranimf 1, 46730 Gandia, Spain
[2] Institut d'Electronique, de Microélectronique et de Nanotechnologie, UMR CNRS 8520, Cité Scientifique, F-59652 Villeneuve d'Ascq Cédex, France
[3] Instituto Universitario de Matemática Pura y Aplicada, Universidad Politécnica de Valencia, Camino de Vera s/n, 46022 Valencia, Spain
E-mail: virogar1@gmail.com

New Journal of Physics **14** (2012) 023049 (21pp)
Received 9 September 2011
Published 21 February 2012
Online at http://www.njp.org/
doi:10.1088/1367-2630/14/2/023049

Abstract. The complex band structures calculated using the extended plane wave expansion (EPWE) reveal the presence of evanescent modes in periodic systems, never predicted by the classical $\omega(\vec{k})$ methods, providing novel interpretations of several phenomena as well as a complete picture of the system. In this work, we theoretically and experimentally observe that in the ranges of frequencies where a deaf band is traditionally predicted, an evanescent mode with excitable symmetry appears, changing drastically the interpretation of the transmission properties. On the other hand, the simplicity of the sonic crystals in which only the longitudinal polarization can be excited is used to interpret, without loss of generality, the level repulsion between symmetric and antisymmetric bands in sonic crystals as the presence of an evanescent mode connecting both repelled bands. These evanescent modes, obtained using EPWE, explain both the attenuation produced in this range of frequencies and the transfer of symmetry from one band to the other in good agreement with both experimental results and multiple scattering predictions. Thus, the evanescent properties of the periodic system have been revealed to be necessary for the design of new acoustic and electromagnetic applications based on periodicity.

[4] Author to whom any correspondence should be addressed.

Contents

1. Introduction

Since the pioneering works of Yablonovitch [1], Yablonovitch and Gmitter [2] and John [3] who simultaneously discovered the possibility of controlling the flow of light in periodic distribution of dielectric materials, there has been significant increasing interest in analogous structures to control both elastic and acoustic waves using the well-known phononic [4, 5] or sonic crystals [6–10], respectively. Phononic crystals are periodic distributions of two elastic materials; however, in the case when one of these materials is a fluid, the system is called a sonic crystal (SC). Over the last 20 years, the exploitation of the particular dispersion relation of these structures has revealed very interesting physical properties [4–33]. The existence of ranges of frequencies, called bandgaps (BGs), in which non-propagating modes can be excited in the system, has been observed in a wide range of frequencies due to the scalability of the systems [13, 14, 28]. The presence of the BGs has motivated the analysis of both the localized states in point defects [11, 12, 15, 17, 22] and the guidance of waves through a linear defect constituting a waveguide in the periodic system [18, 19, 25]. However, other properties of the dispersion relation have been used to control the wave propagation through these periodic structures. On the one hand, the linearity of the dispersion curves at subwavelength regimes has motivated the application of homogenization theories in order to define effective parameters of the system [16, 24]. On the other hand, the curvature of the isofrequency contours has been used to control the spatial dispersion of the waves inside the periodic structures in order to obtain both the self-collimating effect [26, 27] and negative refraction [20, 21].

Recently, the possibility to control the evanescent properties in periodic composites has shown several interesting possibilities in both photonic [35, 36] and phononic [37–39] crystals. Imaging with super-resolution [40, 41], i.e. overcoming the diffraction limit, can be obtained by restoring all the evanescent components of a near-field image. This can be achieved by the coupling of the evanescent modes with other mechanisms leading to their amplification in order to successfully transport the information carried by the evanescent waves through the system. In this way, the evanescent properties of the periodic system have been revealed to be necessary for the design of new acoustic and electromagnetic applications.

The dispersion relation of these periodic structures has been traditionally obtained using $\omega(\vec{k})$ methods, for instance plane wave expansion (PWE) [7]. Using the PWE method, the BGs can be defined as ranges of frequencies in which no modes are excited inside the periodic structure. However, BGs should be defined as ranges of frequencies where only evanescent modes can be excited [42, 43]. Recent works have shown that in both the regimes, acoustic [31] and elastic [44], an extension of the PWE method, called extended plane wave expansion (EPWE), is an efficient tool for analyzing the evanescent properties of periodic systems. This methodology inverts the $\omega(\vec{k})$ problem to the $k(\omega)$ problem by fixing both the angular frequency ω and the direction of incidence $\vec{\alpha}$ ($\vec{k} = k\vec{\alpha}$), k being the eigenvalue of the problem. The supercell approximation has been introduced in EPWE to theoretically characterize the evanescence of both single [30] and double [32] point defects. The evanescent decay predicted by EPWE for both complete and defective SCs is in very good agreement with the experimental measurements [30–32]. The picture of the propagation properties of the periodic systems provided by the EPWE method improves and completes that given by the PWE.

The goal of the paper is twofold. Firstly, we observe the evidence for evanescent modes in a sonic crystal waveguide (SCW) using EPWE with supercell approximation. Secondly, we analyze the evanescent properties of a stubbed SCW. The presence of the stub breaks the symmetry of the system and fundamental phenomena can be studied. The antisymmetry of the system introduces several splittings in the band structure characterized by an interchange of properties between the repelled bands. In this work, we study the nature of the level repulsion in two-dimensional (2D) periodic systems by making use of evanescent waves.

We find the evanescent modes to be of fundamental interest for the correct understanding of wave propagation properties both in linear waveguides and in general structures based on periodicity. We use an SCW because it allows us to obtain high-precision measurements inside the periodic structure where the evanescent properties are excited. As has been previously shown [34], the interest in SCW is in the effects due to the periodicity that cannot exist in rigid wall waveguides. Due to the linear defect in the SCW, interesting physics appear in the BG. In this work, we theoretically and experimentally observe that for the *deaf* bands [9, 45, 46], where the real part of the complex band structure represents antisymmetric modes, evanescent modes with excitable symmetry can appear in the waveguide. In contrast to the classical interpretation of the attenuation in a deaf band, based on geometric arguments, in this work we find that the attenuation is governed by a decay rate related to the imaginary part of the complex band structures obtained using EPWE. Independently, we have obtained the same value of the decay rate using other methodologies, such as multiple scattering theory (MST) [47–50], in very good agreement with the experiments.

On the other hand, mode conversion in a phononic crystal thin slab was recently observed [51]. This conversion depends on the symmetry of the system with respect to the direction of the incident wave. In these systems, the excited modes either couple or not with other ones, the coupling being observed both by a splitting between bands in the band structure and by a transfer of symmetry from one band to the other. In the case when no coupling occurs, the bands simply cross between them. Bavencoffe [52] established a link between the attenuation of the ultrasonic wave observed in the case of a limited grating and the values of the imaginary part of the wave number in a stop band computed for an infinite grating. In other works, Achaoui *et al* [53] recently observed that, in phononic crystals with some freedom of anisotropy, when a band mostly polarized in-plane is close to a band mostly polarized out-of-plane, the phenomenon of repelling can occur and in some instances it introduces a local BG.

Moreover, this interaction is accompanied by a transfer of the polarization state from one band to the other. This level repulsion that avoids crossing in the distribution of eigenvalues is well known within the physics community [54–56]. However, there are only a few works in the literature that analyze and discuss this phenomenon in 2D phononic crystals [51, 53, 57].

The simplicity of the SC in which only the longitudinal polarization can be excited is used to observe without loss of generality the level repulsion between symmetric and antisymmetric bands. In this work, we show that the level repulsion between the symmetric and antisymmetric modes is a result of the presence of an evanescent mode. These evanescent modes explain both the attenuation produced in this range of frequencies and the transfer of symmetry from one band to the other.

The paper is organized as follows. First of all, both the theoretical techniques and the experimental setup are shown in section 2. In section 3, we present the classification of several evanescent modes predicted by the EPWE, showing the main characteristics of the complex band structures of the SCW. The evanescent behavior of modes in the SCW is also analyzed, both analytically using MST and experimentally. Section 4 analyses the stubbed SCW. The evanescent bands, not predicted by the traditional PWE, are very relevant for these systems. The interaction of the evanescent modes with cavity modes in the waveguide is presented in section 4.1. In section 4.2 the stubbed SCW is used to show the effect of level repulsion in periodic systems, showing both the local BGs and the symmetry transfer between symmetric and antisymmetric bands due to the presence of evanescent modes. The concluding remarks will be performed in section 5.

2. Theoretical techniques and the experimental setup

The propagation properties of periodic materials can be analyzed solving for both the eigenvalue and the scattering problems. The former can be used to obtain the dispersion relation of a system, whereas the latter can be used to obtain the scattering of waves in finite structures. Both methodologies are independently used in this work to analyze the properties of an acoustic waveguide. The eigenvalue problem $k(\omega)$ is solved in this work using the EPWE with supercell approximation [32]. To compare the results with the classical $\omega(\vec{k})$ some calculations using the PWE method [7] will be shown. To solve the scattering problem we use the MST [47–50], which is a self-consistent method used to analyze the scattered field of an arrangement of scatterers considering all the orders of scattering.

The experiments shown in this work have been performed in an echo-free chamber sized $8 \times 6 \times 3\,\mathrm{m}^3$. To obtain the experimental dependence of the pressure all along the SCW, we measured the pressure field inside the guide. We built a finite SC hanging the rigid scatterers on a periodic frame (figure 1) and the SCW is generated removing the central row of the complete structure. We note that this system avoids the excess attenuation effect [33]. The finite 2D SC is made of 7×7 rigid cylinders arranged as a square array of the lattice constant a. The radius of the cylinders used in the experiments is $r = 9\,\mathrm{cm}$, and the lattice constant of the SC is $a = 19\,\mathrm{cm}$. With these parameters, the filling fraction of the finite SC is $ff = \frac{\pi r^2}{a^2} \simeq 0.71$. The dimensions of the system are large enough for the microphone to be placed inside the waveguide. The microphone used is a prepolarized free-field $1/2''$ type 4189 B&K. The diameter of the microphone is 1.32 cm, which is approximately $0.07a$; therefore a low level of influence over the pressure field measured is expected. The source is placed 1 m away from the SCW launching white noise.

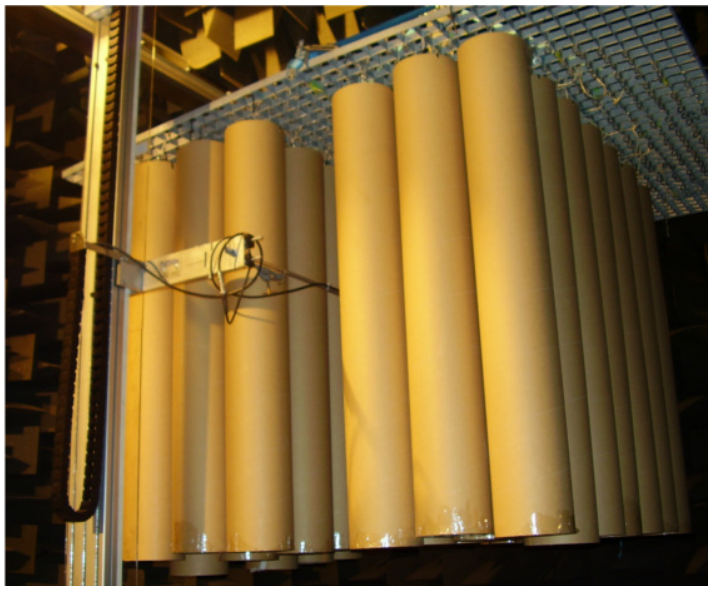

Figure 1. Experimental setup. Picture of the frame in which the SCW has been hung and the complete structure with 7×7 rows in which the central one is removed in order to produce the waveguide.

In this work, a 3D computer-controlled automatic positioning system together with an automatized acquisition system, called the 3D robotized e-acoustic measurement system (3DReAMS), has been used to obtain the pressure field inside the waveguide. The 3DReAMS system is capable of sweeping the microphone through a 3D grid of measuring points located at any trajectory inside the echo-free chamber. The robot was controlled by the motion controller card of National Instruments PCI 7334. We analyzed the acoustic field inside the guide of both the complete SCW and the stubbed SCW by moving the microphone in steps of 1 cm.

3. Propagating and evanescent modes in sonic crystal waveguides

Consider a periodic arrangement of rigid scatterers embedded in air ($\rho_{\text{air}} = 1.29\,\text{kg}\,\text{m}^{-3}$, $c = 340\,\text{m}\,\text{s}^{-1}$) with square periodicity where the lattice constant is a and the filling fraction is $ff = \pi r^2/a^2 = 0.717$. All the physical parameters presented in the work will be shown in reduced magnitudes: reduced frequencies ($\Psi = va/c_{\text{air}}$, where v is the frequency) and reduced Bloch vector ($K = ka/(2\pi)$). The band structure for this periodic array is shown in figure 2(a). The BG of the complete SC (without linear defect) ranges between $\Psi_1 = 0.33$ and $\Psi_2 = 0.8$. In this section, we analyze the evanescent and propagating properties of an SCW generated by removing the central row of the complete structure. EPWE shows novel properties of the guided and non-guided modes in the waveguide that would not be observed otherwise using PWE.

3.1. Preliminary analysis: transmission properties of a sonic crystal waveguide. Motivation

The generated SCW is completely equivalent to that used in a previous work [58]. Figure 2(b) shows the band structure along the ΓX direction for the SCW for these frequencies. The band structure has been calculated using the PWE with the supercell approximation. A total of 1105 plane waves have been used for the calculations. The supercell is shown in the inset of figure 2(b).

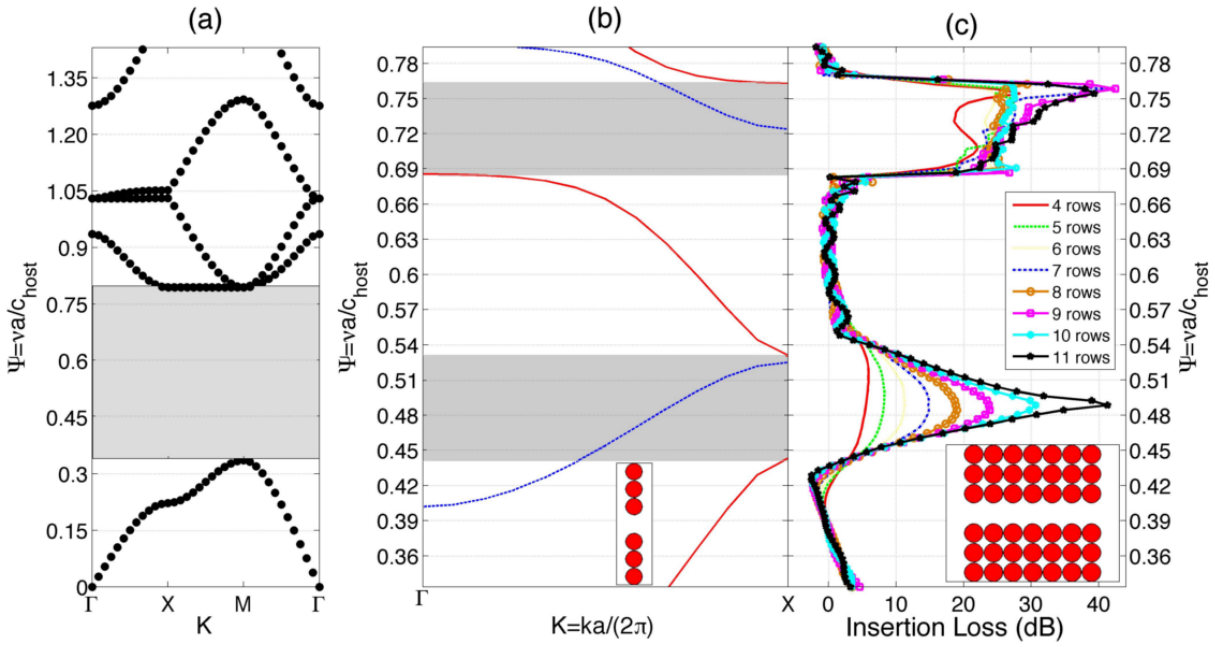

Figure 2. Study of the transmission properties of the SC and SCW. (a) Band structure for the complete SC made of rigid scatterers embedded in air with square periodicity where the lattice constant is a and the filling fraction is $ff = \pi r^2/a^2 = 0.717$. The gray area represents the BG. (b) Band structure of the SCW in the ΓX direction calculated using PWE (1105 plane waves) for the frequencies in the BG of the complete structure. Gray areas represent non-guiding bands. Red continuous (blue dashed) lines represent symmetric (antisymmetric) bands. (c) IL prediction calculated using MST. The different lines represent the IL predictions for the SCW with several rows (see the legend).

Because of the linear defect, the band structure in figure 2(b) shows five guiding bands in the BG. The red continuous and blue dashed lines in figure 2(b) correspond to localized modes in the straight waveguide. The Fourier transform of the eigenvectors yields the pressure field inside the SCW. Analyzing this field [58], one can observe that the modes corresponding to the red continuous lines produce symmetric acoustic fields with respect to the main direction of symmetry ΓX, whereas the acoustic fields corresponding to the blue dashed lines are antisymmetric. Thus the symmetric modes can be excited by a longitudinal incident wave and the antisymmetric modes will not contribute to the transmission because they cannot be excited. The latter modes are usually called *deaf* bands and have been analyzed in the literature [9, 45, 46].

From the previous discussion, it is expected that between symmetric guiding bands there should appear a dip in transmission (gray areas in figure 2(b)). In order to observe this property, one should additionally solve for the scattering problem. We analyze several SCWs with different numbers of rows using MST. We evaluate the insertion loss (IL) [9] which corresponds to the attenuation spectrum evaluating the difference between the sound levels recorded at the same point without and with the SCW. The comparison of the band structure and the IL spectrum shown in figure 2(c) indicates that the symmetric bands (red continuous lines in figure 2(b))

contribute to the transmission, whereas, as was expected, between these symmetric bands, attenuation peaks appear in the IL spectrum because the antisymmetric modes (blue dashed lines in figure 2(b)) cannot be excited.

Figure 2(c) clearly shows the two attenuation peaks produced by the non-excited antisymmetric bands in the waveguide for a large number of rows. However, in the case of a small number of rows the attenuation level due to the first antisymmetric band is very low in comparison with the attenuation level of the second peak (red continuous line in figure 2(c)). Moreover, the attenuation level of the first attenuation peak increases with the number of rows, whereas the second peak seems more stable. Thus, several fundamental questions arise from this plot. First of all, if band structures predict stop bands for these frequencies (gray areas), what kind of modes can propagate depending on the length of the waveguide? Why does the second antisymmetric mode present larger and more stable attenuation levels than the first one? The answers to these questions are related to evanescent waves and cannot be obtained from the results of either the PWE or the MST. A more accurate approach should be used to understand the physics of these systems.

3.2. Complex band structures in sonic crystal waveguides

Brillouin [42] revealed that waves in the BG present evanescent behavior, i.e. the waves should be characterized by a complex value of the wave vector in such a way that the amplitude of the mode should be modulated by an exponential with negative exponent. Therefore the mode should decay as it penetrates the crystal. The elegant and intuitive explanation of Joannopoulos *et al* [43] revealed that the decay rate should be greater for frequencies closer to the center of the BG. Classical methods do not show this kind of property because they interpret the BG as ranges of frequencies where no modes can be excited.

The Joannopoulos predictions have recently been observed both theoretically [31, 44] and experimentally [30, 31] for SCs. Motivated by the properties of the complex band structures and by interesting questions related to evanescent modes presented in the previous section, we study the evanescent and guiding properties of the SCW. The conclusions of this work are general and can be applied to other kinds of periodic systems.

Due to the freedom of the eigenvalues in the EPWE method (complex valued k), a more general band structure than the classical ones is obtained [31, 44]. In this section, we classify the propagating and evanescent modes appearing in the complex band structure resulting from the EPWE method. The classification shown in this work, inspired by the works of Bavencoffe *et al* [52, 59], helps us to understand better the complex band structures. The modes are classified by the following restrictions: (i) The classical band structures correspond to modes characterized by values of $\mathrm{Re}(K)$ in the Brillouin zone and $\mathrm{Im}(K) = 0$. Modes with these properties are shown in this work by black filled circles. (ii) The modes characterized by $\mathrm{Im}(K) \geqslant 0$ and $\mathrm{Re}(K) = 0$ are shown by red filled triangles. These modes represent connections between propagating bands at the Γ-point. (iii) The modes characterized by $\mathrm{Im}(K) \geqslant 0$ and $\mathrm{Re}(K) = 1/2$ (respectively, $\mathrm{Re}(K) = 1/\sqrt{2}$) are shown by green filled squares. These modes represent connections between propagating bands at the X (respectively, M) point. (iv) The modes with $\mathrm{Re}(K)$ in the first Brillouin zone but with $\mathrm{Im}(K) \neq 0$ are shown by blue filled diamonds. These modes belong to evanescent connecting bands between bands with the same symmetry of the acoustic field. For this last group, we constrain the plots for modes with $\mathrm{Im}(K) \leqslant 0.4$.

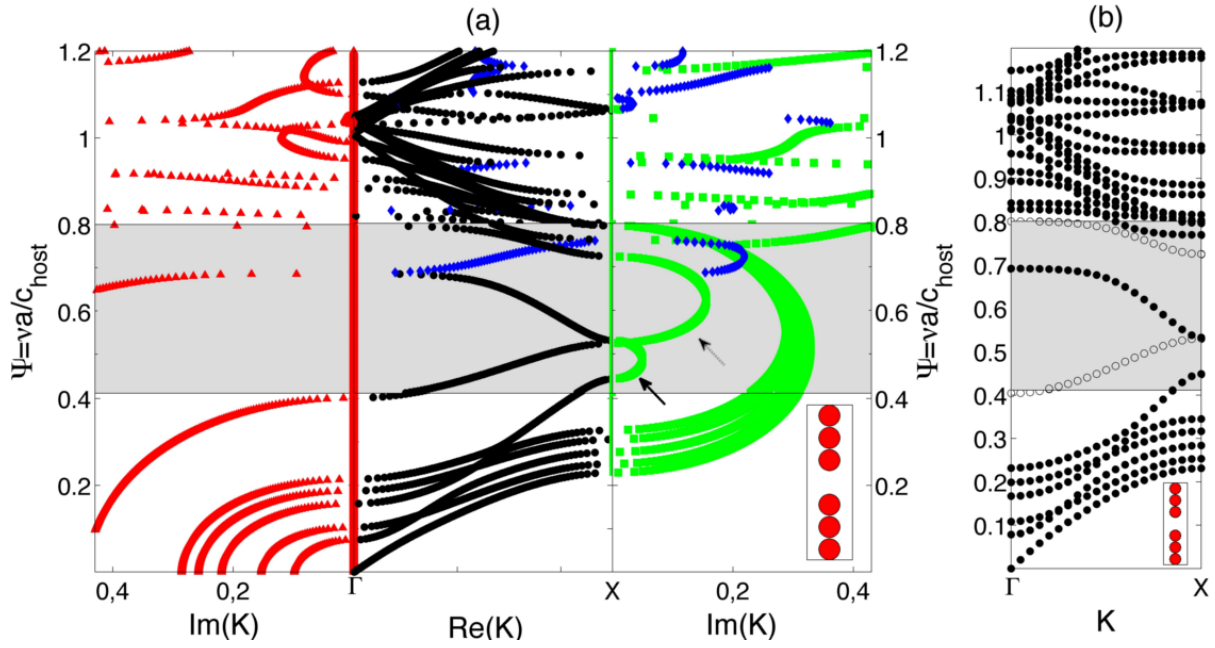

Figure 3. Analysis of the band structure of the SCW. The gray area represents the BG. Reduced magnitudes have been used in the plots. (a) Calculation using EPWE. Red triangles represent modes with $\mathrm{Im}(K) \neq 0$ and $\mathrm{Re}(K) = 0$; black circles represent modes with $\mathrm{Re}(K) \neq 0$ and $\mathrm{Im}(K) = 0$; green squares show modes with $\mathrm{Re}(K) = 0.5$ and $\mathrm{Im}(K) \neq 0$ and blue diamonds represent modes with $0 < \mathrm{Re}(K) < 0.5$ and $\mathrm{Im}(K) \neq 0$. (b) Band structure calculated using PWE. Inside the BG, open circles (black circles) represent antisymmetric (symmetric) modes. The supercells used in both cases are shown in the insets of (a) and (b).

Following the previous classification, we have plotted the complex band structure calculated using the EPWE with supercell approximation for the SCW we are dealing with. The convergence of all the calculations has been carefully analyzed selecting an adequate number of plane waves for each case. A total of 1369 plane waves have been used for the calculation. Figure 3(a) shows the complex band structure for the SCW in the ΓX direction. The values of the real part of the wave vector (the central panel of figure 3(a)) are restricted to the first Brillouin zone, whereas the imaginary part (right and left panels of figures 3(a)) is arbitrarily displayed. It is worth noting that due to the frequency discretization to solve the EPWE, it is difficult to find flat bands in the band structure. Thus, the frequency step used in this work has been specifically selected for each calculation. The gray area shows the range of frequencies of the BG of the perfect complete SC. The supercell used for the calculations is shown in the inset of figure 3(a).

Comparing the band structures calculated using EPWE and PWE in figures 3(a) and (b), respectively, one can observe that EPWE reproduces the same guided modes in the BG as in the case of PWE. However, two important characteristics should be noted. Firstly, the complex band structure shows that two consecutive symmetric (respectively, antisymmetric) real bands are connected by a symmetric (respectively, antisymmetric) imaginary band indicated with the black continuous (respectively, dotted) arrow in figure 3(a). Therefore, the complex connections

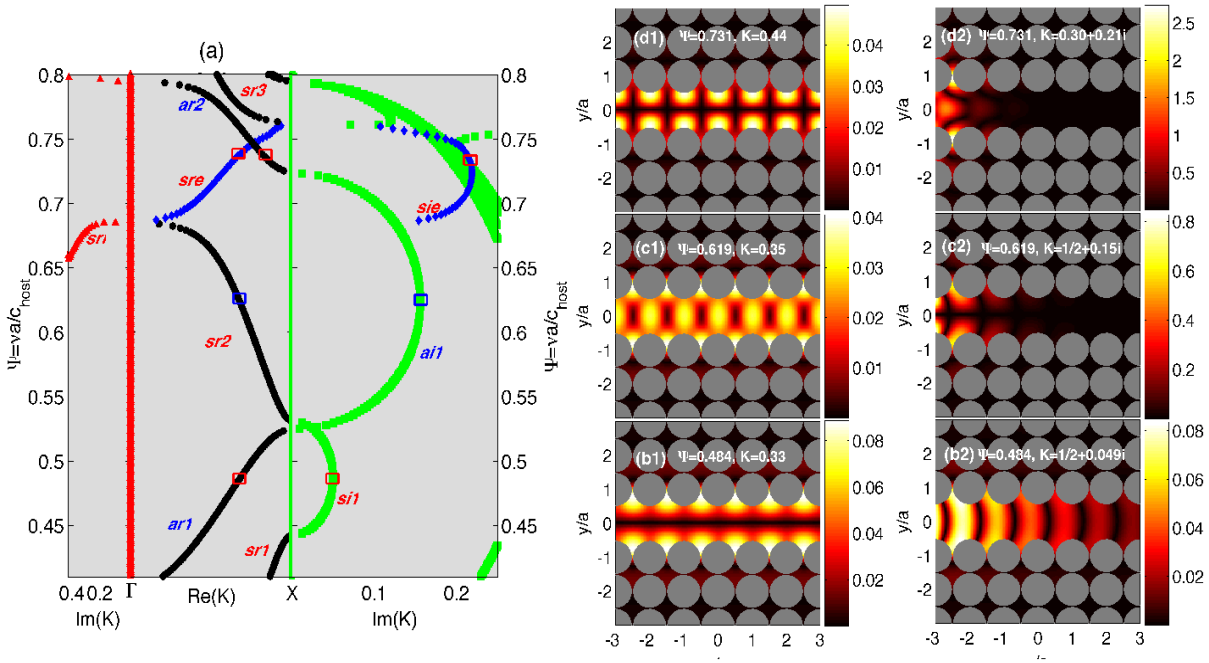

Figure 4. Analysis of the propagating and evanescent modes of the SCW predicted by EPWE (modes at $\Psi = 0.484$, $\Psi_2 = 0.619$ and $\Psi_3 = 0.731$). (a) Complex bands in the BG region. (b1)–(d1) Modulus of the acoustic field for the real eigenvalues. (b2)–(d2) Modulus of the acoustic field for the complex eigenvalues.

preserve the symmetry of the bands which are connecting. Secondly, as a consequence of the connections and due to the folding of the bands, an additional band not predicted by PWE appears in the BG (see real and imaginary bands indicated with blue diamonds). Let us analyze these two features in detail.

At Γ or X points where the folding of the bands is expected, an evanescent connection between the bands should appear to preserve the overall number of bands at any frequency. In order to observe this, we fix our attention on the BG for the complete periodic system. Figure 4(a) shows the complex band structure for this range of frequencies. Let us analyze the first symmetric (respectively, antisymmetric) guided band labeled as *sr1* (*ar1*) in figure 4(a). Note that this band is connected to the second symmetric (antisymmetric) band, *sr2* (respectively, *ar2*), by means of a complex band with a non-zero imaginary part *si1* (*ai1*). It is worth noting that both the maximum value of the band *sr1* (*ar1*) and the minimum value of the *sr2* (*ar2*) are at the point X. Thus the complex band that connects these two symmetric (antisymmetric) real bands presents a constant value of the real part, whereas the imaginary part follows a connecting path between the two real bands preserving the symmetry of the band.

In the range of frequencies between the two symmetric (antisymmetric) bands, PWE predicts that due to the antisymmetry (symmetry) of the acoustic field, stop (guiding) bands are expected. Here, between the symmetric bands *sr1* and *sr2*, an evanescent symmetric band, *si1*, is excited, whereas between the two antisymmetric bands *ar1* and *ar2*, a symmetric real band is excited, *sr2*. Thus, the interpretation of EPWE gives a complete picture of the physics

of the problem. The stop bands can be interpreted as ranges of frequencies where symmetric evanescent modes are excited, the decay rate of the mode inside the SCW being linked to the imaginary part of the complex wave vector.

To interpret these results we have selected two different modes at two different frequencies, one at $\Psi_1 = 0.484$ ($K_1 = 1/2 + 0.049\mathrm{i}$) and the other at $\Psi_2 = 0.619$ ($K_2 = 0.35$). The analyzed modes are marked in the band structure in figure 4(a) with red squares. For the analysis, we only select the first complex band because the complex bands with high values of $\mathrm{Im}(K)$ do not contribute to the transmission properties of the SCW. Figures 4(b1) and (b2) (4(c1) and (c2)) show the acoustic field of the mode for the real and complex eigenvalues at the frequency Ψ_1 (Ψ_2), respectively. The acoustic field has been obtained from the Fourier transform of the eigenvectors for the corresponding frequency. We would like to note that the real mode at the band *ar1* (*sr2*) is exactly the same as that predicted using PWE with a value of $K = 0.33$ ($K_2 = 0.35$) presenting the antisymmetric (symmetric) acoustic field. In contrast, the complex mode only predicted by EPWE at the band *si1* (*ai1*) is characterized by a value of the Bloch vector $K_1 = 1/2 + 0.049\mathrm{i}$ ($K = 1/2 + 0.15\mathrm{i}$) with a symmetric (antisymmetric) evanescent acoustic field. Thus, because of the symmetry of the SCW, only the modes with a symmetric acoustic field are excited. Therefore, for the frequency Ψ_1 the stop band is characterized by the evanescent mode shown in figure 4(b2), whereas for the frequency Ψ_2 the symmetric propagating mode shown in figure 4(c1) is expected.

The connection between the bands *sr2* and *sr3* is different from that in the previous cases. The maximum value of the band *sr2* is at the Γ point, whereas the minimum value of the band *sr3* is at the X point. Then, the evanescent connection between these bands presents both a real part that crosses the path ΓX, *sre*, and an imaginary part, *sie*, connecting the bands in the imaginary part. This connection produces an additional band that has never been predicted by PWE. To analyze this situation we have selected two modes at the frequency $\Psi_3 = 0.731$, one with a real value of the Bloch vector, $K = 0.44$, at band *ar2* and another with a complex value of the Bloch vector, $K_3 = 0.33 + 0.21\mathrm{i}$, being the real part of K in the band *sre* and the imaginary part in the band *sie*. The acoustic fields of the real and complex modes are shown in figures 4(d1) and (d2), respectively. One can observe that the acoustic field corresponding to the real mode, shown in figure 4(d1), is antisymmetric and cannot be excited in the SCW. However, the evanescent field produced by the complex mode (figure 4(d2)), shows a symmetric acoustic field and, as a consequence, is an excitable mode in the SCW.

The EPWE predictions allow us to affirm that the two stop bands in the SCW (gray areas in figure 2(b)) are characterized by two evanescent symmetric modes. The first stop band is characterized by an evanescent band that presents lower values of the imaginary part than in the case of the second stop band. This feature explains both the dependence of the IL spectra on the number of rows and the stability of the attenuation level of the second peak shown in figure 2(c). However, due to the assumption of periodicity, the EPWE predictions are for an infinite SCW. In order to both check and clarify the previous results we have calculated the acoustic fields in a real waveguide made of a complete SC of 11×11 rows in which we have created a linear defect in the central column (columns are defined in the direction of incidence).

Figure 5 shows the MST calculation for the three frequencies previously analyzed: (a) $\Psi_1 = 0.484$, (b) $\Psi_2 = 0.619$ and (c) $\Psi_3 = 0.731$. Figures marked with 1's show the absolute value of the acoustic pressure field inside the waveguide, whereas the figures labelled with 2's show the longitudinal cut of the field inside the waveguide for $y/a = 0$. The MST calculation predicts acoustic fields inside the waveguide similar to the symmetric ones obtained from the

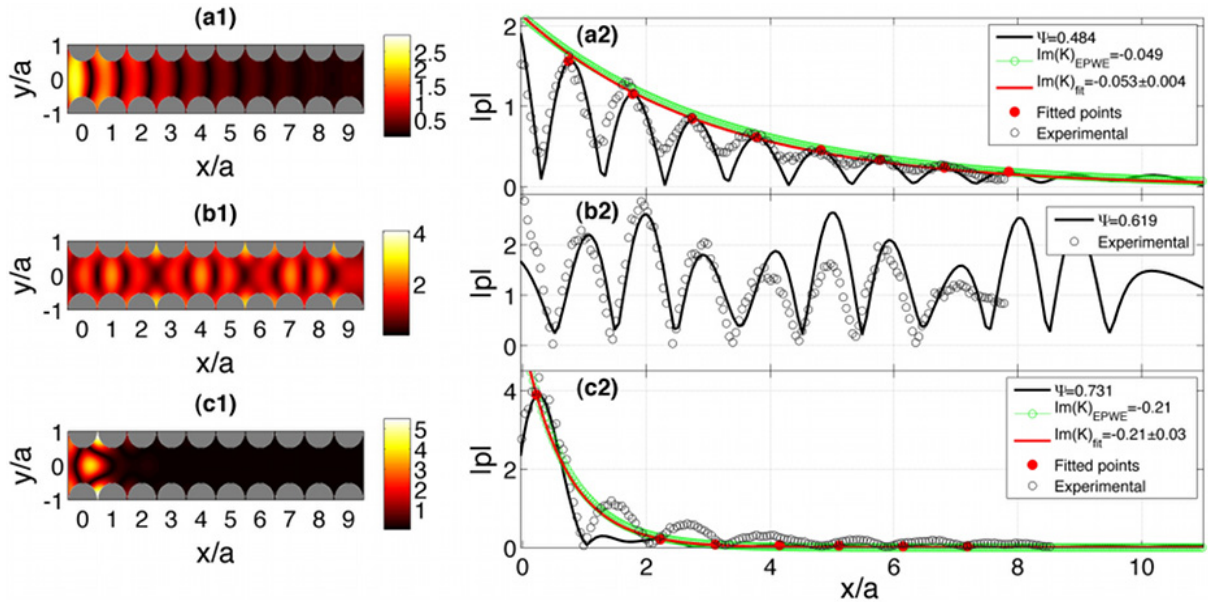

Figure 5. Multiple scattering analysis of the excited modes in a waveguide made by removing one row of scatterers located at $y/a = 0$ in an SC constituted by 10×10 cylinders. (a1)–(a2), (b1)–(b2) and (c1)–(c2) show the acoustic field inside the waveguide and the longitudinal cut at $y = 0$ (black continuous line) for frequencies 0.484, 0.619 and 0.713, respectively. The red line shows the exponential fit of the red circles that represents the decay of the mode. The green line represents the decay predicted using $\mathrm{Im}(K)$ from EPWE. Open black circles represent the measurements in the experimental setup (see section 2).

Fourier transform of the eigenvectors of the EPWE for the analyzed frequencies. This means that the excited acoustic field in the SCW corresponds to the first symmetric mode predicted by EPWE. Thus, the mode at $\Psi = 0.619$ should propagate through the waveguide, whereas the modes at $\Psi = 0.484$ and $\Psi = 0.731$ should be evanescent and the decay should be comparable with the value of the imaginary part of the K.

To analyze both the propagating and the evanescent behavior of modes, we study the acoustic field in the longitudinal cut at $y/a = 0$. Figure 5(b2) represents the cut corresponding to the propagating mode at $\Psi = 0.619$. One can observe that the field does not present any decay and the wave is guided through the waveguide. In contrast, figures 5(a2) and (c2) present the cuts for the evanescent modes at 0.484 and 0.731. These cuts clearly show the decay produced because of the evanescent nature of the excited mode. The experiments (open black circles) are in good agreement with the evanescent behavior of the modes.

In order to check that effectively the excited modes in the stop bands correspond to the evanescent mode obtained using EPWE, we have fitted the decay of the modes to an exponential $a\,\mathrm{e}^{-bx}$. The fit of the mode at $\Psi = 0.484$ using the maximum points shown in figure 5(a2) by red circles gives a value of the decay rate $\mathrm{Im}(K)_{\mathrm{fit}} = 0.053 \pm 0.004$. This value is in complete agreement with that predicted by EPWE, $\mathrm{Im}(K) = 0.049$. On the other hand, an analogous procedure gives a decay rate for the mode at $\Psi = 0.731$ equal to $\mathrm{Im}(K)_{\mathrm{fit}} = 0.21 \pm 0.03$, in complete agreement with the $\mathrm{Im}(K) = 0.21$ (figure 5(c2)) predicted by EPWE.

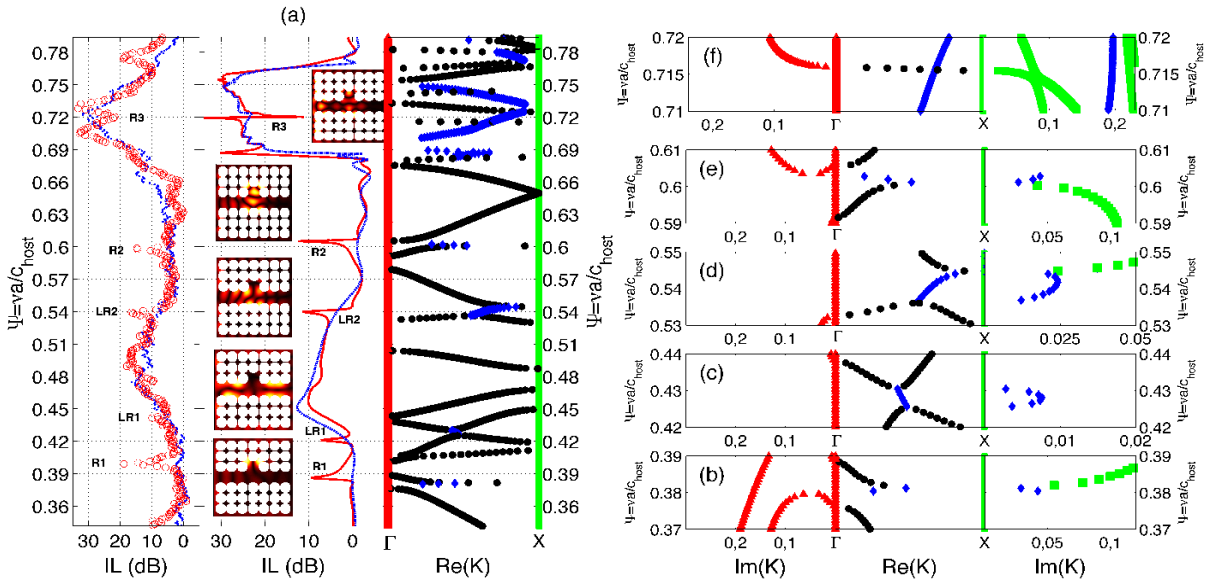

Figure 6. Theoretical and experimental analyses of the stubbed waveguide using EPWE and MST. (a) The IL spectrum evaluated at the end of the waveguide. In the central panel, the blue continuous line (red dashed line) represents the MST predictions, and in the left panel, blue dots (open red circles) represent the experimental results of the SCW (stubbed SCW). Peaks labelled as R (LR) represent the effect of resonances of the stub (the effect of the level repulsion between bands with different symmetries). The right panel presents the real part of the complex band structure for the SCW. Panels (b)–(f) show details of both the hybridization of the resonances and the guide or evanescent modes and the repulsion between bands (see text).

4. Evanescent coupling and level repulsion states in sonic crystal waveguides

The interaction between stubs or point defects with waveguides has been extensively analyzed in the literature [34, 58, 60]. The presence of the stub or a defect in an SCW alters drastically the transmission spectrum. Although the general characteristics of the transmission properties of the SCW are preserved once the stub or the defect is created in the waveguide, narrow attenuation peaks appear in the guided bands occurring at the resonance modes of the stub. The stub modes are evanescent and strongly localized by the surrounding periodic structure.

In this section, we investigate both theoretically and experimentally the occurrence of effects produced by a stub in an SCW. Stubs are generated in this work by removing a scatterer in the side wall of the waveguide. We observe two different effects due to the stub. On the one hand, EPWE predicts attenuation dips due to the interaction of both the guided and the evanescent modes with the resonances of the stub. This result constitutes a proof of the importance of the $k(\omega)$ methods because they predict the evanescent bands and, as a consequence, the interaction between the evanescent modes and the resonances of the stub. The attenuation peaks in figure 6(a) marked with R (resonance) correspond to this first effect and will be discussed in detail later.

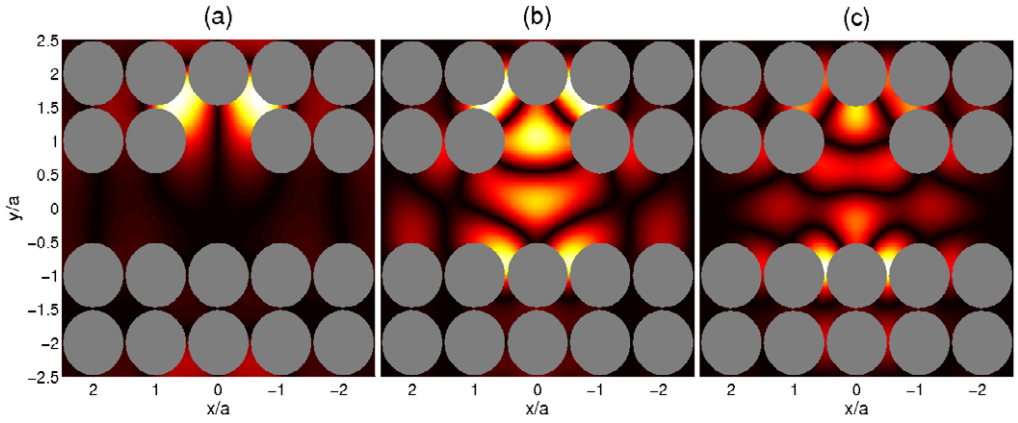

Figure 7. Absolute value of the acoustic field for the stub resonances. (a) R1, $\Psi_1 = 0.3812$; (b) R2, $\Psi_2 = 0.605$; (c) R3, $\Psi_3 = 0.72$.

On the other hand, the presence of the stub changes the symmetry of the system; therefore antisymmetric modes can be excited even by symmetric longitudinal incident waves. This causes the appearance of repulsion states between symmetric and antisymmetric bands. In this work, we observe that due to the local breaking of the symmetry because of the presence of the stub, a repelling state appears between symmetric and antisymmetric bands accompanied by a transfer of the symmetry of the modes from one band to the other. Chen *et al* [51] showed that depending on the symmetry of the system with respect to the direction of the incident wave, shear-horizontal modes either couple or not with the Lamb wave modes which are polarized in the sagittal plane. The coupling can be observed by a splitting between bands in the band structure and by a transfer of the symmetry from one band to the other. In the case when no coupling occurs, the symmetric Lamb wave band simply crosses the shear-horizontal band. Similar results have recently been observed in 1D phononic crystals [52, 59] and anisotropic phononic crystals [53]. We observe in this work a new interpretation: the repelled bands are connected by an evanescent mode which is responsible for the transfer of symmetry from one band to another. The attenuation peaks in figure 6(a) marked with LR (level repulsion) correspond to this second effect and will be discussed in detail later.

The real part of complex band structures of the stubbed waveguide is also shown in the right panel of figure 6(a). One can observe the correspondence between the attenuation peaks, R and LR, predicted by MST (the central panel of figure 6(a)) and the singular points of the band structure. The left panel of figure 6(a) shows the experimental data (see section 2 for details of the experimental setup) in good agreement with the theoretical predictions. Let us study the nature of each of these attenuation peaks.

4.1. Coupling between guided and evanescent modes with stub resonances

The stub acts as a resonant cavity in the waveguide producing flat bands due to the localized mode in the stub. If this resonance occurs at the same frequency as a guiding or evanescent band, then the hybridization of the two bands produces an attenuation peak in the spectrum. Resonances of the stub, calculated using EPWE at the point X, can be observed in figure 7. It is worth noting that the frequencies of these resonances coincide with two symmetric guiding bands and one evanescent band of the waveguide.

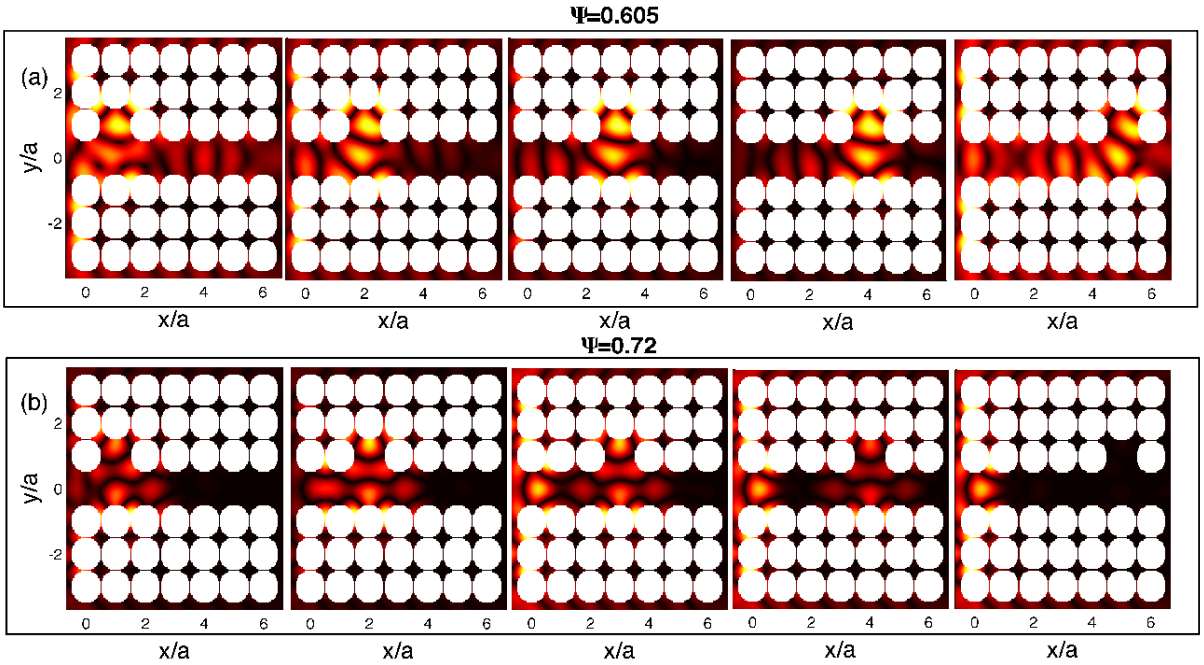

Figure 8. Coupling of guided and evanescent modes with stub resonances. (a) Coupling of the resonance at $\Psi = 0.605$ with the guided mode at the same frequency. (b) Coupling of the resonance at $\Psi = 0.72$ with the evanescent mode at the same frequency.

Points R1 ($\Psi = 0.3812$) and R2 ($\Psi = 0.605$) in figure 6(a) coincide with the hybridization of the guiding bands and the resonance bands of the stub (flat band). A detailed image of the hybridization effect at these frequencies can be seen in figures 6(b) and (e). These hybridizations explain the attenuation peaks in the IL spectrum labelled as R1 and R2 in figure 6(a), in good agreement with both the analytical predictions and the experimental results. The shape of the attenuation peaks resembles the Fano-like resonances reported previously [61]. The slight disagreement between the experimental data and the theoretical predictions may be due to the sensitivity of the experimental data to the size of the stub.

The interaction between the guided mode in the SCW and the resonance of the stub at point R2 is analyzed in figure 8(a). The calculations have been performed using the MST. We study the propagation of waves at the frequency $\Psi = 0.605$ inside an SCW $7a$ long with a stub. The position of the stub has been changed all along the SCW in order to observe that the guided mode excites the resonance of the stub independently of the distance between the site of the stub and the entrance of the SCW (left side of the SCW). The wave penetrates the waveguide exciting the symmetric guided mode. Once the guided mode finds the stub, the resonance of the stub is excited, localizing the field in that region. One can compare the field around the stub in figure 8(a), calculated using MST, with the acoustic field of the resonance of the stub in figure 7(b) calculated using EPWE. It is worth noting that the resonance of the stub is excited practically with the same intensity at all the locations of the stub due to the low losses of the guided mode. An analogous effect occurs for the point R1 ($\Psi = 0.3812$).

The point R3 ($\Psi = 0.72$) corresponds to the interaction of an evanescent mode with the resonance of the stub at this frequency. The detailed band structure for this frequency is shown

in figure 6(f). Note that for this case no hybridization is produced and two bands can be excited. Once the wave penetrates the SCW the evanescent mode is excited and, if the stub is as close as the evanescent mode can travel through the SCW, the stub mode should be excited. Note that these results are not predicted by the classical methods; therefore they cannot be explained with the PWE, but EPWE gives the correct understanding of the phenomenon.

MST simulations have been carried out in order to observe this coupling between the evanescent mode and the stub resonances at $\Psi = 0.72$. Figure 8(b) shows five stubbed waveguides with increasing distances between the sites of the stub and the entrance of the SCW. In all cases, the excited evanescent mode presents a symmetric acoustic field equivalent to that predicted by EPWE in figure 4(d2). Once this mode arrives at the stub, it excites the stub resonance. However, it is worth noting that the mode is evanescent and, as a consequence, the intensity of the localized modes in the stub should decrease as the stub is farther from the entrance of the SCW. The MST calculations predict this behavior. For the last case, the distance between the stub and the entrance of the SCW is longer than the penetration distance of the evanescent mode and, as a consequence, any stub resonance can be excited.

4.2. Level repulsion states

In addition to the attenuation peaks due to the resonances, the IL spectrum of the stubbed waveguide (figure 6(a)) predicts two additional attenuation peaks referred to as LR1 ($\Psi = 0.429$) and LR2 ($\Psi = 0.544$). These peaks have a different phenomenology than R1, R2 or R3 peaks, which are due to the interaction between the guided or evanescent modes with the stub resonances (see the previous section). In contrast, the LR1 and LR2 peaks correspond to crossing points in the band structure shown in figure 6(b).

Very recent works [53] have shown several kinds of crossing points in anisotropic phononic crystals. As a general rule for these systems, the bands involved in the crossing point, or level repulsion state, exchange their polarization, so that the polarization remains a continuous function of the wave vector $\vec{k}$. For the case of SC in which only longitudinal polarization is allowed, one can observe symmetric and antisymmetric acoustic fields. If the SC is symmetric with respect to the incident acoustic field, only symmetric acoustic fields will be supported. However, if the system is non-symmetric, then both symmetric and antisymmetric fields can be supported. The stubbed SCW is an example of a non-symmetric system.

In our case, the points LR1 and LR2 correspond to level repulsion states in the band structures that introduce a local BG. The level repulsion state for these cases appears due to the crossing between an antisymmetric and a symmetric band in a similar way as in phononic crystal thin plates [51, 52, 59]. Figures 6(c) and (d) present detailed views of the band structures calculated using EPWE for the points LR1 and LR2, respectively. One can see that, in both cases, the repelled bands are connected by means of an additional band, which is evanescent. Thus, EPWE does not predict a repulsion level state but an evanescent connection between bands.

In order to analyze in more detail the phenomenology involved in these level repulsion states, we have analyzed several modes for different frequencies all along the bands involved in the repulsion. Figure 9 shows the acoustic fields obtained from the Fourier transform of the eigenvectors for several modes in the repelled bands. The analyzed modes are marked with red squares, which are connected using red arrows with their corresponding acoustic fields.

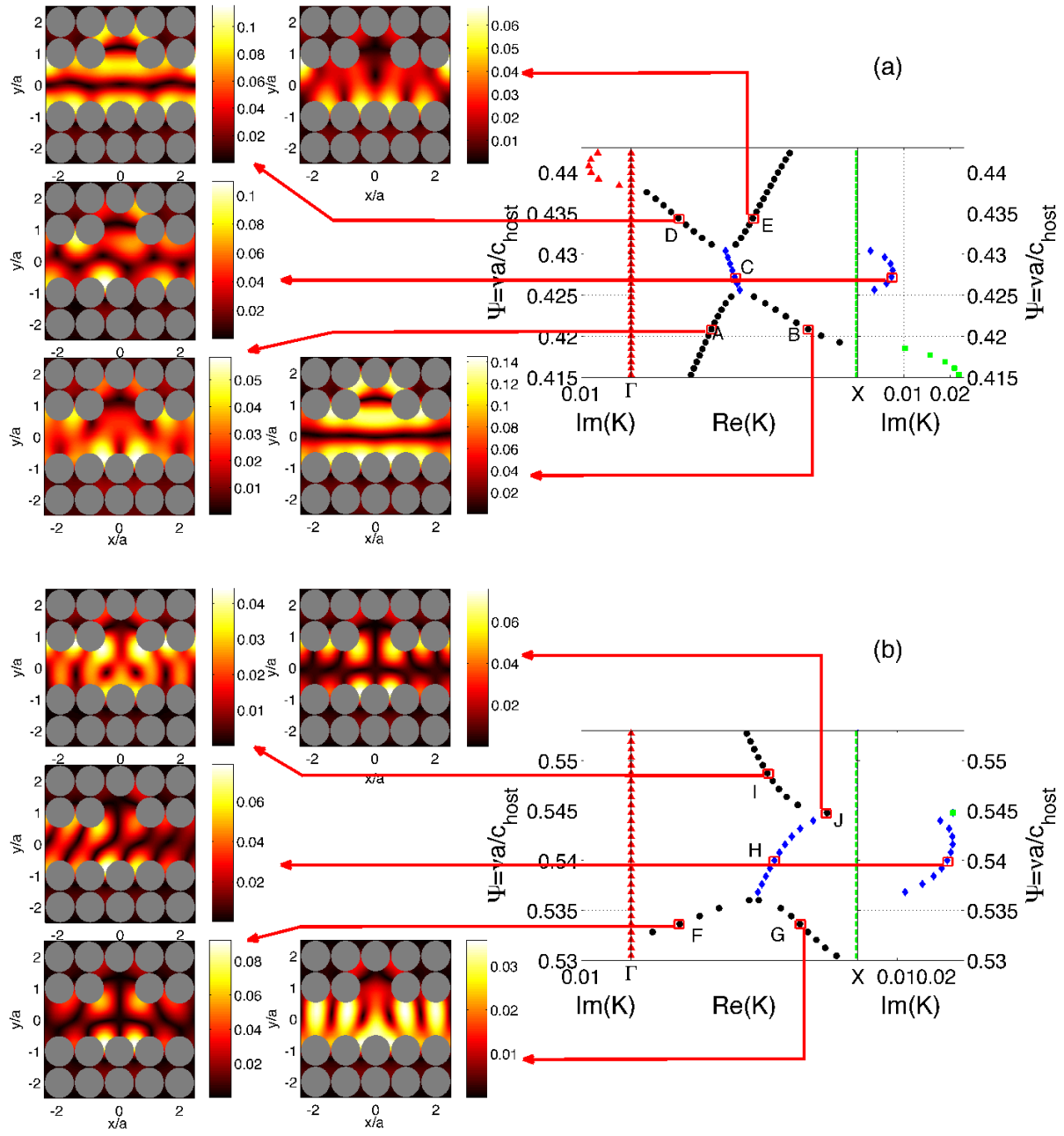

Figure 9. Analysis of the symmetry transfer between the repelled bands in stubbed waveguides. The analysis in (a) and (b) corresponds to the repulsion states shown in figures 6(f) and (e), respectively. The acoustic fields are represented using the absolute value of the pressure obtained from the Fourier transform of the eigenvectors for the eigenvalues marked with red squares.

One can observe that the modes in the repelled bands present a completely real eigenvalue, k, whereas the connection bands have a complex eigenvalue. The repelled bands are predicted by EPWE and are exactly the same as those predicted by the PWE; however, the difference appears in the evanescent connection between the repelled bands.

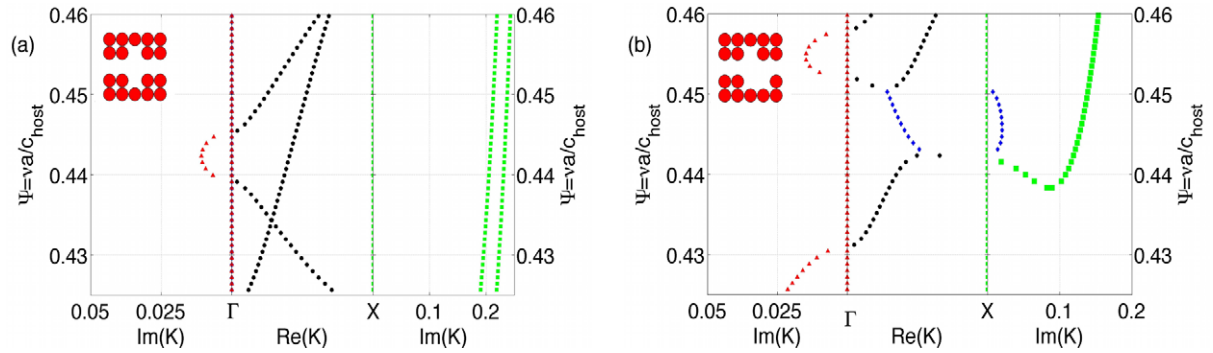

Figure 10. Complex band structures of two stubbed SCWs, one symmetric (a) and the other antisymmetric (b). The supercells for the EPWE calculations are shown in the insets. The evanescent connection between the repelled bands is marked with blue diamonds for the case of the antisymmetric stubbed SCW.

First, we fix our attention on the acoustic fields in the repelled bands. One can observe in figure 9 that for each band, depending on the position with respect to the evanescent connection, different symmetries of the field can be excited. For example, points A and B that belong to the same band have different symmetries. A is on the left of the evanescent connection and B is on the right of the evanescent connection. The acoustic field corresponding to the point A is mainly symmetric. However, the acoustic field for the point B is completely antisymmetric. Then, inside the band, there is an exchange of the symmetry, so that the symmetry remains a continuous function of the wave vector $\vec{k}$ for each band. The same situations appear for the couples of modes D–E, F–G and I–J.

The repelled bands are connected by an evanescent band which is responsible for the exchange of symmetry between bands. The acoustic fields of the modes inside the evanescent connection have mixed symmetry. We have studied modes C and H in the evanescent connections. First of all, one can see the mixed symmetry of the acoustic field for modes C and H. Moreover, one can observe the evanescent behavior of the acoustic field inside the guide with a low decay rate indicating the small value of the imaginary part of the eigenvalue, k. It is worth noting that the acoustic field predicted by MST for the frequencies corresponding to modes C and H is fairly close to that predicted by EPWE (figure 8). The MST predictions can be seen in figure 6(a).

4.2.1. Symmetric and antisymmetric stubbed sonic crystal waveguides. Following the previous results, the repulsion states in SCs should appear in systems presenting some degree of antisymmetry, such as for example a stubbed SCW. For the sake of clarity of the previous results, we have analyzed two additional systems, a symmetric one and another with a degree of antisymmetry. Figure 10(a) shows the complex band structure for a completely symmetric system with a symmetric stub as shown in the inset. Figure 10(b) shows the complex band structure for the SCW with an antisymmetric stub whose supercell is also shown in the inset.

One can observe that the band structure of the symmetric stubbed SCW presents a crossing point but the bands are not connected, i.e. they are independent and only the symmetric one will contribute to the transmission properties of the system. However, for the case of the antisymmetric stubbed SCW one can observe again the evanescent connection between the repelled bands (blue diamonds).

5. Concluding remarks

The complex band structures obtained using the EPWE ($k(\omega)$ method) show additional bands never revealed by the classical $\omega(\vec{k})$ methods. In this work, we have shown both theoretically, with two independent theoretical techniques (EPWE and MST), and experimentally, making use of 3DReAMS, the interpretation of these evanescent additional bands. Due to the conservation of the overall number of bands for a determined frequency, interesting interpretations of the deaf bands and the level repulsion states have been obtained depending or not on the symmetry of the system. In the ranges of frequencies where a deaf band is traditionally predicted an evanescent mode with excitable symmetry appears, changing drastically the transmission properties of the system. On the other hand, we have interpreted, without loss of generality, the level repulsion between symmetric and antisymmetric bands in antisymmetric sonic crystal stubbed waveguides as the presence of an evanescent mode connecting both bands. These evanescent modes explain both the attenuation produced in this range of frequencies and the transfer of symmetry from one band to the other. Thus, the additional bands of EPWE are not an artifact of the calculation but real physical behavior can be attributed to them and, as a consequence, the evanescent modes should be considered in the design of systems based on periodicity.

Acknowledgments

VRG and LMGR are grateful for the hospitality and the facilities provided by the Institut d'Electronique, de Microélectronique et de Nanotechnologie (IEMN UMR CNRS 8520). LMGR thanks the Universidad Politécnica de Valencia for the grant 'Programa de Apoyo a la Investigación y Desarrollo (PAID-00-11)'. VRG is grateful for the support provided by 'Programa de Contratos Post-Doctorales con Movilidad UPV (CEI-01-11)'. This work was supported by MCI Secretaría de Estado de Investigación (the Spanish government) and FEDER funds under grant no. MAT2009-09438.

References

[1] Yablonovitch E 1987 Inhibited spontaneous emission in solid-state physics and electronics *Phys. Rev. Lett.* **58** 2059

[2] Yablonovitch E and Gmitter T J 1989 Photonic band structures: the face-centered-cubic case *Phys. Rev. Lett.* **63** 1950

[3] John S 1987 Strong localization of photons in certain disordered dielectric superlattices *Phys. Rev. Lett.* **58** 2486

[4] Sigalas M and Economou E N 1993 Band structure of elastic waves in two dimensional systems *Solid State Commun.* **86** 141

[5] Kushwaha M S, Halevi P, Dobrzynski L and Djafari-Rouhani B 1993 Acoustic band structure of periodic elastic composites *Phys. Rev. Lett.* **71** 2022–5

[6] Martínez-Sala R, Sancho J, Sánchez J V, Gómez V, Llinares J and Meseguer F 1995 Sound attenuation by sculpture *Nature* **378** 241

[7] Kushwaha M S, Halevi P, Martiñez G, Dobrzynski L and Djafari-Rouhani B 1994 Theory of acoustic band structure of periodic elastic composites *Phys. Rev.* B **49** 2313–22

[8] Kushwaha M S 1997 Stop-bands for periodic metallic rods: sculptures that can filter the noise *Appl. Phys. Lett.* **70** 3218

[9] Sánchez-Pérez J V , Caballero D, Martínez-Sala R, Rubio C, Sánchez-Dehesa J, Meseguer F, Llinares J and Gálvez F 1998 Sound attenuation by a two-dimensional array of rigid cylinders *Phys. Rev. Lett.* **80** 5325–8

[10] Robertson W M and Rudy J F III 1998 Measurement of acoustic stop bands in two-dimensional periodic scattering arrays *J. Acoust. Soc. Am.* **104** 694–9
[11] Sigalas M M 1997 Elastic wave band gaps and defect states in two-dimensional composites *J. Acoust. Soc. Am.* **101** 1256
[12] Sigalas M M 1998 Defect states of acoustic waves in a two dimensional lattice of solid cylinders *J. Appl. Phys.* **84** 3026
[13] Caballero D, Sánchez-Dehesa J, Rubio C, Martínez-Sala R, Sánchez-Pérez J V, Meseguer F and Llinares J 1999 Large two-dimensional sonic band gaps *Phys. Rev.* E **60** R6316
[14] Tanaka Y, Tomoyasu Y and Tamura S 2000 Band structure of acoustic waves in phononic lattices: two-dimensional composites with large acoustic mismatch *Phys. Rev.* B **62** 7387–93
[15] Wu F G, Hou Z L, Liu Z Y and Liu Y Y 2001 Point defect states in two-dimensional phononic crystals *Phys. Lett.* A **292** 198
[16] Cervera F, Sanchis L, Sánchez-Pérez J V, Martínez-Sala R, Rubio C and Meseguer F 2002 Refractive acoustic devices for airborne sound *Phys. Rev Lett.* **88** 023902–4
[17] Wu F, Zhong H, Zhong S, Liu Z and Liu Y 2003 Localized states of acoustic waves in three-dimensional periodic composites with point defects *Eur. Phys. J.* B **34** 265–8
[18] Khelif A, Choujaa A, Djafari-Rouhani B, Wilm M, Ballandras S and Laude V 2003 Trapping and guiding of acoustic waves by defect modes in a full-band-gap ultrasonic crystal *Phys. Rev.* B **68** 214301
[19] Khelif A, Wilm M, Laude V, Ballandras S and Djafari-Rouhani B 2004 Guided elastic waves along a rod defect of a two-dimensional phononic crystal *Phys. Rev.* E **69** 067601
[20] Yang S, Page J H, Liu Z, Cowan M L, Chan C T and Sheng P 2004 Focusing of sound in a 3D phononic crystal *Phys. Rev. Lett.* **93** 024301
[21] Feng L, Liu X P, Chen Y B, Huang Z P, Mao Y W, Chen Y F, Zi J Z and Zhu Y Y 2005 Negative refraction of acoustic waves in two-dimensional sonic crystals *Phys. Rev.* B **72** 033108
[22] Li X and Liu Z 2005 Coupling of cavity modes and guiding modes in two-dimensional phononic crystals *Solid State Commun.* **133** 397–402
[23] Sigalas M, Kushwaha M S, Economou E N, Kafesaki M, Psarobas I E and Steurer W 2005 Classical vibrational modes in phononic lattices: theory and experiment *Z. Kristallogr.* **220** 765–809
[24] Torrent D, Hakansson A, Cervera F and Sánchez-Dehesa J 2006 Homogenization of two-dimensional cluster of rigid rods in air *Phys. Rev. Lett.* **96** 204302
[25] Tanaka Y, Yano T and Tamura S I 2007 Surface guided waves in two-dimensional phononic crystals *Wave Motion* **44** 501–12
[26] Pérez-Arjona I, Sánchez-Morcillo V J, Redondo J, Espinosa V and Staliunas K 2007 Theoretical prediction of the nondiffractive propagation of sonic waves through periodic acoustic media *Phys. Rev.* B **75** 014304
[27] Espinosa V, Sánchez-Morcillo V J, Staliunas K, Pérez-Arjona I and Redondo J 2007 Subdiffractive propagation of ultrasound in sonic crystals *Phys. Rev.* B **76** 140302
[28] Vasseur J O, Deymier P A, Djafari-Rouhani B, Pennec Y and Hladky-Hennion A C 2008 Absolute forbidden bands and waveguiding in two-dimensional phononic crystal plates *Phys. Rev.* B **77** 085415
[29] Pennec Y, Vasseur J O, Djafari-Rouhani B, Dobrzynski L and Deymier P A 2010 Two-dimensional phononic crystals: examples and applications *Surf. Sci. Rep.* **65** 229–91
[30] Romero-García V, Sánchez-Pérez J V, Castiñeira Ibáñez S and Garcia-Raffi L M 2010 Evidences of evanescent Bloch waves in phononic crystals *Appl. Phys. Lett.* **96** 124102
[31] Romero-García V, Sánchez-Pérez J V and Garcia-Raffi L M 2010 Evanescent modes in sonic crystals: complex dispersion relation and supercell approximation *J. Appl. Phys.* **108** 044907
[32] Romero-García V, Sánchez-Pérez J V and Garcia-Raffi L M 2010 Propagating and evanescent properties of double-point defects in sonic crystals *New J. Phys.* **12** 083024
[33] Romero-García V, Sánchez-Pérez J V and Garcia-Raffi L M 2011 Analytical model to predict the effect of a finite impedance surface on the propagation properties of 2D sonic crystals *J. Phys. D: Appl. Phys.* **44** 265501

[34] Khelif A, Djafari-Rouhani B, Vasseur J O, Deymier P A, Lambin Ph and Dobrzynski L 2002 Transmittivity through straight and stublike waveguides in a two-dimensional phononic crystal *Phys. Rev.* B **65** 174308
[35] Li X, He S and Jin Y 2007 Subwavelength focusing with a multilayered Fabry–Perot structure at optical frequencies *Phys. Rev.* B **75** 045103
[36] Dong J W, Zheng H H, Lai Y, Wang H and Chan C T 2011 Metamaterial slab as a lens, a cloak, or an intermediate *Phys. Rev.* B **83** 115124
[37] Sukhovich A, Merheb B, Muralidharan K, Vasseur J O, Pennec Y, Deymier P A and Page J H 2009 Experimental and theoretical evidence for subwavelength imaging in phononic crystals *Phys. Rev. Lett.* **102** 154301
[38] Robillard J F, Bucay J, Deymier P A, Shelke A, Muralidharan K, Merheb B, Vasseur J O, Sukhovich A and Page J H 2011 Resolution limit of a phononic crystal superlens *Phys. Rev.* B **83** 224301
[39] Zhu J, Christensen J, Jung J, Martin-Moreno L, Yin X, Fok L, Zhang X and Garcia-Vidal F J 2011 A holey-structured metamaterial for acoustic deep-subwavelenght imaging *Nat. Phys.* **7** 52–5
[40] Pendry J B 2000 Negative refraction makes a perfect lens *Phys. Rev. Lett.* **85** 3966
[41] Fang N, Lee H, Sun C and Zhang X 2005 Sub-diffraction-limited optical imaging with a silver superlens *Science* **308** 534
[42] Brillouin L 1946 *Wave Propagation in Periodic Structures* (New York: McGraw-Hill)
[43] Joannopoulos J D, Johnson S G, Winn J N and Meade R D 2008 *Photonic Crystals Molding the Flow of Light* (Princeton, NJ: Princeton University Press)
[44] Laude V, Achaoui Y, Benchabane S and Khelif A 2009 Evanescent Bloch waves and the complex band structure of phononic crystals *Phys. Rev.* B **80** 092301
[45] Rubio C, Caballero D, Sánchez-Pérez J V, Martínez-Sala R, Sánchez-Dehesa J, Meseguer F and Cervera F 1999 The existence of full gaps and deaf bands in two-dimensional sonic crystals *J. Lightwave Technol.* **17** 2202
[46] Hsiao F L, Khelif A, Moubchir H, Choujaa A, Chen C C and Laude V 2007 Complete band gaps and deaf bands of triangular and honeycomb water–steel phononic crystals *J. Appl. Phys.* **101** 044903
[47] Martin P A 2006 *Multiple Scattering. Interaction of Time-Harmonic Waves with N Obstacles* (Cambridge: Cambridge University Press)
[48] Linton C M and McIver P 2001 *Handbook of Mathematical Techniques for Wave/Structure Interactions* (Boca Raton, FL: CRC Press)
[49] Chen Y Y and Ye Z 2001 Theoretical analysis of acoustic stop bands in two-dimensional periodic scattering arrays *Phys. Rev.* E **64** 036616
[50] Kafesaki M and Economou E N 1999 Multiple scattering theory for three-dimensional periodic acoustic composites *Phys. Rev.* B **60** 11993
[51] Chen J J, Bonello B and Hou Z L 2008 Plate-mode waves in phononic crystal thin slabs: mode conversion *Phys. Rev.* E **78** 036609
[52] Bavencoffe M 2009 *PhD Thesis* University of Le Havre
[53] Achaoui Y, Khelif A, Benchabane S and Laude V 2010 Polarization state and level repulsion in two-dimensional phononic crystals and waveguides in the presence of material anisotropy *J. Phys. D: Appl. Phys.* **43** 185401
[54] Dembowski C, Graf H D, Harney H L, Heine A, Heiss W D, Rehfeld H and Richter A 2001 Experimental observation of the topological structure of exceptional points *Phys. Rev. Lett.* **86** 787
[55] Philipp M, von Brentano P, Pascovici G and Richter A 2000 Frequency and width crossing of two interacting resonances in a microwave cavity *Phys. Rev.* E **62** 1922
[56] Lee G, SamKim J and Zak J 2003 Numerical verification of topological crossings in band structure of solids *J. Phys.: Condens. Matter* **15** 2005
[57] Wu T T and Huang Z G 2004 Level repulsions of bulk acoustic waves in composite materials *Phys. Rev.* B **70** 214304

[58] Vasseur J O, Deymier P A, Beaugeois M, Pennec Y, Djafari-Rouhani B and Prevost D 2005 Experimental observation of resonant filtering in a two-dimensional phononic crystal waveguide *Z. Kristallogr.* **220** 829

[59] Bavencoffe M, Morvan B, Izbicki J L and Hladky-Hennion A C 2009 Characterization of evanescent ultrasonic waves in a band gap of a 1D phononic crystal *Ultrasonics, IEEE Int. Symp.* p 1024

[60] Benchabane S, Khelif A, Choujaa A, Djafari-Rouhani B and Laude V 2005 Interaction of waveguide and localized modes in a phononic crystal *Europhys. Lett.* **71** 570–5

[61] Goffaux C, Sánchez-Dehesa J, Yeyati A L, Lambin Ph, Khelif A, Vasseur J O and Djafari-Rouhani B 2003 Evidence of Fano-like interference phenomena in locally resonant materials *Phys. Rev. Lett.* **88** 225502